FRET Detection of Cellular α_4-Integrin Conformational Activation

Alexandre Chigaev,* Tione Buranda,* Denise C. Dwyer,* Eric R. Prossnitz,† and Larry A. Sklar*
*Department of Pathology and Cancer Center, and †Department of Cell Biology and Physiology, University of New Mexico Health Sciences Center, Albuquerque, New Mexico

ABSTRACT Integrins are cell adhesion receptors, expressed on every cell type, that have been postulated to undergo conformational changes upon activation. Here, different affinity states were generated by exposing α_4-integrins to divalent ions or by inside-out activation using a chemokine receptor. We probed the dynamic structural transformation of the integrin on live cells using fluorescence resonance energy transfer (FRET) between a peptide donor, which specifically binds to the α_4-integrin, and octadecyl rhodamine B acceptors incorporated into the plasma membrane. We analyzed the data using a model that describes FRET between a random distribution of donors and acceptors in an infinite plane. The distance of closest approach was found to vary with the affinity of the integrin. The change in distance of closest approach was ~50 Å between resting and Mn^{2+} activated receptors and ~25 Å after chemokine activation. We used confocal microscopy to probe the lateral organization of donors and acceptors subsequent to integrin activation. Taken together, FRET and confocal results suggest that changes in FRET efficiencies are primarily due to the vertical extension of the integrin. The coordination between the extension of α_4-integrin and its affinity provides a mechanism for Dembo's catch-bond concept.

INTRODUCTION

Integrins are cell surface receptors, expressed by all multicellular animals, that mediate cell-matrix, cell-cell, and cell-pathogen interactions. Integrins participate in a large number of physiological processes including tissue morphogenesis, inflammatory recruitment of leukocytes, blood coagulation, wound healing, and others (Humphries, 2000; Hynes, 1992; Shimaoka et al., 2002). A remarkable feature of integrins in comparison to other adhesion molecules is that their ability to bind ligand can be regulated by intracellular signaling. Regulation of integrin function can be evaluated by changes in the avidity (adhesive properties) of a cell (Shimaoka et al., 2002). Several different mechanisms, including rapid change in the conformation (affinity modulation), clustering, and association with cytoskeletal elements have been proposed to explain the functional responses (Bazzoni and Hemler, 1998; Diamond and Springer, 1994; Dustin and Springer, 1989; Faull et al., 1994; Loftus et al., 1994; Stewart and Hogg, 1996; Van Kooyk et al., 1999).

Over the last decade, conformational changes within integrin family members have been detected using mAbs that recognize activation-dependent epitopes (Lu et al., 2001; Bazzoni and Hemler, 1998), electron microscopy with $\alpha_{IIb}\beta_3$-integrin (Du et al., 1993), or using the change in the affinity for ligand of the α_4-integrin (Chen et al., 1999b). Cell activation may also lead to changes in the topography of integrins on the cell surface (Bazzoni et al., 1998). In electron micrographs, integrin molecules ($\alpha_5\beta_1$, $\alpha_{IIb}\beta_3$) appeared as a round headpiece on a long stalk region (Nermut et al., 1988; Du et al., 1993; Takagi et al., 2001). X-ray crystallography of $\alpha_V\beta_3$ revealed a bent conformation, in which the headpiece is folded over the tailpiece and each integrin "leg" is bent at its "knee" (Xiong et al., 2001). It has been proposed that an "unusual flexibility" of the molecule "may be linked to integrin regulation" (Xiong et al., 2001). A nuclear magnetic resonance study of the Cys-rich module-3 of the integrin β_2 subunit (not resolved by crystal structure) and the subsequent modeling of the I-EGF domains of $\alpha_V\beta_3$ have demonstrated that epitopes for mAbs that are buried in the bent conformation become exposed after activation of the integrin (Beglova et al., 2002). Based on such data, it has been proposed that the bent conformation represents an inactive integrin state and that activation is accompanied by a "switchblade-like" opening of the integrin (Shimaoka et al., 2002; Beglova et al., 2002).

The $\alpha_4\beta_1$-integrin is unique among the leukocyte integrins in that it supports both rolling and firm adhesive interactions (Alon et al., 1995; Chen et al., 1999a). The relationship between the molecular affinity for ligands, the adhesive avidity for cell attachment, molecular conformation, and lateral organization is therefore of particular interest for this integrin class. An adhesion-dependent conversion among states of different avidity has been previously predicted for integrins from theoretical considerations and described as the catch-bond concept (Dembo et al., 1988). This work represents the first systematic attempt to evaluate the relationship between integrin affinity and conformation on live cells, using fluorescence techniques to resolve vertical and lateral contributions.

Here, we used flow cytometry and fluorescence resonance energy transfer (FRET) to probe the dynamic structural transformation of the integrin in response to divalent cations and cell stimulation. We used a fluorescent peptide derivative that specifically binds to α_4-integrin (Chigaev et al., 2001) as a donor and octadecyl rhodamine B (R18) as an acceptor. We

Submitted February 27, 2003, and accepted for publication August 14, 2003.

Alexandre Chigaev and Tione Buranda contributed equally to this work.

Address reprint requests to Prof. Larry A. Sklar, Dept. of Pathology and Cancer Center, University of New Mexico HSC, Albuquerque, NM 87131. Tel.: 505-272-6892; Fax: 505-272-6995; E-mail: lsklar@salud.unm.edu.

0006-3495/03/12/3951/12 $2.00

interpreted acceptor surface density, and transfer in terms of separation distances (Wolber and Hudson, 1979). We found that the separation distance between the binding sites of the integrin molecule and membrane surface depends on the affinity state of the integrin, generated using divalent cations. Replacing Ca^{2+} with Mn^{2+} resulted in an apparent extension of ~50 Å. In addition, the human monoblastoid cell line U937 transfected with wild-type and mutant formyl peptide receptor (Kew et al., 1997) showed an effect of ''inside-out'' signaling on integrin conformation. The changes in the efficiency of FRET and affinity were intermediate to the maximal ion-induced changes, and the time course of these changes coincided with the dynamics of the affinity changes described elsewhere (Chigaev et al., 2001, 2003). With confocal microscopy we verified that the lateral distribution of the integrin and the acceptor molecules was not detectably altered by any of the cell treatments.

MATERIALS AND METHODS

Cell lines and transfectant construct

The human monoblastoid U937 cell line was purchased from ATCC (Rockville, MD). Site-directed mutants of formyl peptide receptor (FPR) in U937 cells were prepared as described (Kew et al., 1997).

Probes for FRET

Octadecyl rhodamine B chloride (R18) and 5-octadecanoylaminofluorescein (F18) were from Molecular Probes (Eugene, OR).

Fluorescently labeled peptides

The α_4 specific peptide derivative (Chen et al., 1999a,b) 4-((*n*′-2-methylphenyl)ureido)-phenylacetyl-L-leucyl-L-aspartyl-L-valyl-L-prolyl-L-alanyl-L-alanyl-L-lysine (LDV peptide derivative) and its FITC-conjugated analog were synthesized at Commonwealth Biotechnologies (Richmond, VA). fNle-Leu-Phe-Nle-Tyr-Lys-Alexa633 was synthesized as follows. Alexa Fluor 633 carboxylic acid succinimidyl ester (Molecular Probes) and fNle-Leu-Phe-Nle-Tyr-Lys (Sigma, St. Louis, MO) were each dissolved in anhydrous dimethyl sulfoxide to 2 mM. Equal volumes were incubated at room temperature overnight with 100 mM TEA and the product used without further purification.

Flow cytometry

Cell- and bead-based fluorescence measurements were performed on a Becton-Dickinson FACScan flow cytometer (Sunnyvale, CA) interfaced to a Power PC Macintosh using the CellQuest software package. The FACScan is equipped with a 15-mW air-cooled argon ion laser. The laser output is fixed at 488 nm.

Equilibrium binding of LDV-FITC to $\alpha_4\beta_1$-integrins on cells

The detailed analysis of LDV-FITC binding was described previously (Chigaev et al., 2001, 2003). Cells were treated with a range of concentrations of the fluorescent ligand (typically 0–12 nM) in the presence of divalent cations (1 mM Mn^{2+}, 1 mM Mn^{2+} +1 mM Ca^{2+}, and 1 mM Ca^{2+}). Nonspecific binding was determined using 500-fold excess unlabeled peptide. All experiments were performed in HEPES buffer (110 mM NaCl, 10 mM KCI, 10 mM glucose, 1 mM $MgCl_2$, and 30 mM HEPES, pH 7.4) containing 0.1% HSA. U937 cells were used at a density of 1×10^6 cells/ml). Incubations have been performed for short times at 37°C and overnight on ice with qualitatively similar results. Analysis was performed on the FACScan by acquiring 5000–10,000 events. Thus, mean channel fluorescence (MCF) values for specific and nonspecific binding were obtained for each ligand concentration; the difference between the two, (ΔMCF) represents specific binding. Dissociation constants (K_d) were calculated using a single site (hyperbolic) binding equation from measurements of the site concentration, site occupancy, and free ligand (curve fits were performed using GraphPad Prism (San Diego, CA). It is worth noting that calibration methods are available to convert MCF into site numbers (Chigaev et al., 2003).

Kinetic analysis of binding and dissociation

Kinetic analysis was done as described previously (Chigaev et al., 2001, 2003). Briefly, cells (1×10^6 cells/ml) were preincubated in HEPES buffer with the specified concentrations of divalent cations for 10–30 min at 37°C. Samples were analyzed for 30–120 s to establish a baseline, then the fluorescent ligand was added, and FACS acquisition was immediately re-established, losing 5–10 s of the total time course. The resulting data were converted to mean channel fluorescence over time using FACSQuery software developed by Bruce Edwards.

Fluorescence resonance energy transfer

General considerations

Fluorescence resonance energy transfer (FRET) is a distance-dependent interaction between the electronic excited states of two chromophores in which excitation is transferred from an excited donor (D^*) molecule (e.g., fluorescein) to an acceptor (A) molecule (e.g., rhodamine) without emission of a photon. The characteristic distance at which the donor fluorescence and FRET are equally probable is defined as R_0. On a surface, the efficiency of FRET is determined from the reduction in the emission quantum yield of the donor according to Eq. 1, where Q_D refers to the emission yield of the donor in the absence of acceptors, and Q_{DA} refers to the donor emission yield in the presence of acceptors expressed in terms of acceptors per unit area as acceptors/R_0^2 (Wolber and Hudson, 1979),

$$E = 1 - \frac{Q_{DA}}{Q_D}. \quad (1)$$

R_0 is calculated according to

$$\mathbf{R}_0 = (JQ_D\kappa^2/n^4)^{1/6}(9.79 \times 10^3 \text{Å}), \quad (2)$$

where J is the donor-acceptor spectral overlap in $cm^3\ M^{-1}$ and n is the refractive index (1.333) of the medium. κ^2 is the dipole-dipole orientation factor (usually taken as 2/3) (Lakowicz, 1999). However, for randomized static orientations of donors and acceptors, $\kappa^2 = 0.476$. In the case of LDV-FITC immobilized by VLA-4 and R18 embedded in the membrane, a combination of dynamic and static factors are likely in place.

Energy transfer in two dimensions

Energy transfer data were analyzed by expressions that describe energy transfer between random distributions of donors and acceptors on lipid membrane surfaces (Dewey and Hammes, 1980; Doody et al., 1983; Fung and Stryer, 1978; Sklar et al., 1980; Wolber and Hudson, 1979). We have used two approaches that will be described below. The first approach (Wolber and Hudson, 1979) involves the calculation of the distance of

closest approach (r_c) between randomly distributed donors and acceptors on an infinite plane and is described by a simple series approximation, as

$$\frac{Q_{DA}}{Q_D} = A_1 e^{-k_1 c} + A_2 e^{-k_2 c}, \quad (3)$$

where

$$c = acceptors/R_0^2, \quad (4)$$

and where $R_0 = 55$ Å (Haugland, 2002). The values of A_1, k_1, A_2, and k_2 were taken from Table 1 in Wolber and Hudson and correspond to the exact solution to the series approximation for different values of r_c expressed as a function of R_0. It is important to note that the values of k_2 for $r_c/R_0 = 1.1$ and 1.3 in the original reference (Wolber and Hudson, 1979) have been recently corrected from 0.4654 and 0.5633, to 0.04654 and 0.005633, respectively (see Table 15.2 in Lakowicz, 1999). This approach is valid for $0 < c < 0.5$ and when the distance of closest approach is $<1.3\ R_0$. Outside this range FRET is significantly overestimated. Thus the second approach of Dewey and Hammes is complementary to the Wolber and Hudson method in that it can be used to account for energy transfer in the range spanning $0.7\ R_0 < r_c < 2\ R_0$ (Dewey and Hammes, 1980). The formulation of Dewey and Hammes assumes that donors and acceptors are uniformly distributed on parallel planes, separated by a distance L. However, the possibility of an excluded volume around the donor is not accounted for, thus L is nominally equivalent to the distance of closest approach (r_c) in Eq. 3. Because the limiting values of r_c examined in this work were on the order of R_0 or less, the data were analyzed using the Wolber and Hudson approach. Thus the Dewey and Hammes method will not be discussed further, although it is worth noting that, for similar ranges of $1 \leq R_0$ and $0.5 \leq c$, these methods give similar results.

FRET experimental design

The excited state donors used in this work are the LDV-FITC peptide and F18, whereas the acceptor is R18. The effective use of these probes in our experiments requires that they have similar spectral characteristics, so as to yield similar values of R_0. The values of R_0 for the set of donor-acceptor pairs used here were derived from calculation of the overlap integral J in buffer solution. The respective values of J were of the same magnitude (1.57×10^{-13} cm^{-3} M^{-1}). The derived values of R_0 were determined to be 52 and 55 Å, for $\kappa^2 = 0.476$ and 0.667, respectively.

To characterize the distance of closest approach between the integrin headgroup and the lipid membrane, we used the α_4 specific ligand, LDV-FITC, as a FRET donor with octadecyl rhodamine B chloride (R18) lipophilic probe as an acceptor. U937 cells were preincubated with 50–100 nM LDV-FITC. Samples were incubated with different concentrations of R18 (up to 20 μM) for 1 min and then donor intensities were measured using the FACScan flow cytometer at 37°C. To characterize lateral energy transfer on the cells we used 5-octadecanoylaminofluorescein (F18) as the donor probe (1 μM, 1-min incubation time). The surface calibration experiments were performed at temperatures at <15°C to minimize the uptake of the donor (F18) probe and were performed in parallel with 1 mM Ca^{2+} LDV-FITC treated cells.

TABLE 1 Summary of rate constants for LDV-FITC obtained for the different affinity states in equilibrium (K_d) and dissociation (k_{off}) experiments

Affinity state	K_d, nM	k_{off}, s^{-1}
1 mM Mn^{2+} + 3 mM DTT*	–	0.0003
1 mM Mn^{2+}	0.14	0.0006
1 mM Mn^{2+} + 1 mM Ca^{2+}	2.8	0.0048
1 mM Ca^{2+}	36	0.07
100 nM fMLFF	5–9	0.02†

*3 mM DTT, 40 min, 37°C.

†The dissociation rate k_{off} for the formyl peptide-stimulated U937 cells transfected with formyl peptide receptor was determined previously (Chigaev et al., 2001).

For real-time FRET experiments, U937 cells were stably transfected with the wild-type or the nondesensitizing mutant (ΔST) of the formyl peptide receptor. The U937 cells were preincubated with 50–100 nM LDV-FITC (to saturate low affinity sites of the integrin) in HHB buffer containing 1.5 mM $CaCl_2$ and 1 mM $MgCl_2$. Flow cytometric analysis was performed continuously for up to 1000 s. Samples were analyzed for 60–120 s to establish a baseline, then saturating R18 (10 μM final) was added to yield maximal quenching. One minute after R18 was added, fMLFF peptide (0.1 μM) was added. FACS acquisition was immediately re-established, losing 5–10 s of the total time course. The cells were also tested using low (3–5 nM) concentration of LDV-FITC to determine the affinity change (Chigaev et al., 2001).

Confocal microscopy

U937 cells were washed once with 0.5 mM EDTA and resuspended in preheated (37°C) HEPES buffer containing 0.1% HSA and the specified concentrations of divalent cations. A total of 2×10^6 cells/ml were stained for 5–15 min at 37°C with 50–100 nM LDV-FITC or 1–5 min with 1 μM R18. The control sample was removed and immediately fixed in ice-cold 2% paraformaldehyde. For activation experiments cells were stimulated with 20 nM fNle-Leu-Phe-Nle-Tyr-Lys-Alexa633 peptide (Molecular Probes). Samples were collected at 0, 30, 180, and 300 s after addition of the formyl peptide and immediately fixed with 2% ice-cold paraformaldehyde then stored overnight at 4°C. The following day cells were washed with ice-cold PBS and resuspended in Vectashield (Vector Laboratories, Burlingame, CA). Fluorescence microscopy was performed with confocal microscope (Zeiss 510 Laser Scanning Microscope) using the 63× 1.4 DIC oil immersion objective lens, and laser excitation at 488, 543, and 633 nm. The surface distribution of receptors and fluorescent molecules was quantified with LSM 510 image analysis software. Minimal fluorescence was detected when cells were unstained or blocked with 500-fold excess of the unlabeled LDV peptide derivative.

RESULTS

Different affinity states of the integrin detected using small fluorescent ligand

Different affinity states of the integrin were generated using combinations of divalent cations or using inside-out signaling through G-protein coupled receptors (see Integrin Conformation is Regulated by Inside-Out Signaling). States of different affinity for the LDV-peptide exhibit homogeneous dissociation rate constants indicative of individual conformations (Table 1 and (Chigaev et al., 2001). This ligand competes for the same binding site as the natural ligand (Chigaev et al., 2001; Chen et al., 1999b). Mn^{2+} is usually used to generate a high affinity state while Ca^{2+} stabilizes a low affinity conformation (Chen et al., 1999b; Hu et al., 1996; Humphries, 1996; Mould et al., 1995). We used three different combinations of Ca^{2+} and Mn^{2+} (1 mM Mn^{2+}, 1 mM Mn^{2+} + 1 mM Ca^{2+}, and 1 mM Ca^{2+}) to generate different affinities of the integrin as described in Materials and Methods (see Equilibrium Binding of LDV-FITC to $\alpha_4\beta_1$-Integrins on Cells; and Kinetic Analysis of

Binding and Dissociation). With this protocol we were able to generate affinity states which spanned >2 orders of magnitude in the affinity of the α_4-integrin as measured by LDV-FITC binding and dissociation (Table 1). The dissociation constants (K_d) were from 0.14 nM in a buffer containing 1 mM Mn^{2+} to 36 nM in a buffer containing 1 mM Ca^{2+}. The dissociation rates (k_{off}) ranged from 0.0006 s^{-1} to 0.07 s^{-1}, respectively. Having thus established the conditions necessary for the generation of several affinity states from equilibrium binding and dissociation experiments, we turned to FRET measurements to characterize the conformational state associated with a given affinity state.

The distance of closest approach between the integrin ligand binding site (LDV-FITC) and the cell membrane probes (R18) depends on the affinity state of the integrin

Fig. 1 shows a schematic representation of the lateral organization of plasma membrane, probes, and receptors. Shown in the scheme is an integrin $\alpha\beta$ heterodimer that is inactive and bent over, with the two cytoplasmic domains closely apposed. Upon activation the integrin assumes an extended upright conformation. Energy transfer between lipophilic probes and the integrins bearing fluorescent ligands provides a way of characterizing changes in the conformational state of the integrin, including any concomitant changes in the lateral organization of the plasma membrane. The fluorescent peptide (LDV-FITC) specifically binds to the α_4-integrin as a fluorescent donor and octadecyl rhodamine B (R18) lipophilic probe functions as an acceptor. Addition of octadecyl rhodamine B (R18) leads to the incorporation of the lipid acceptor into the cell membrane, which results in FRET between the LDV-FITC peptide and R18. The efficiency of FRET was shown to depend on the affinity state of the integrin.

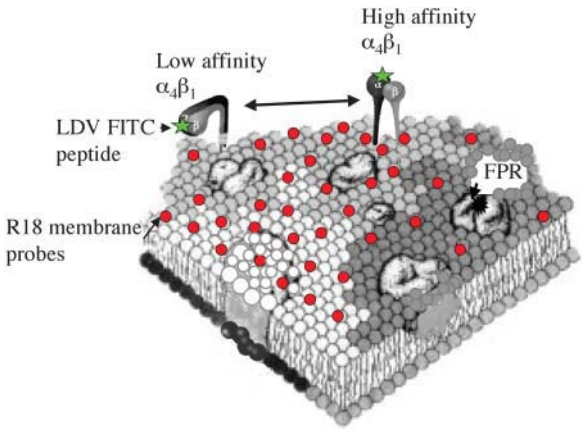

FIGURE 1 Lateral organization of cellular plasma membrane and receptors. An integrin $\alpha\beta$ heterodimer that is inactive and is bent over, with the two cytoplasmic domains closely apposed. Upon activation the integrin assumes an extended upright conformation. When activated, the formyl peptide receptor is known to aggregate in punctate microdomains believed to be lipid rafts. Energy transfer between lipid probes and receptors bearing fluorescent ligands provides a way of studying lateral organization and integrin conformation. The fluorescent peptide derivatives (LDV-FITC) binds to the α_4-integrin as a fluorescent donor. Octadecyl rhodamine B (R18), a lipophilic probe, inserts into the membrane as an acceptor. (Adapted from Vaz and Melo, 2001.)

Fig. 2 shows the quenching of donor fluorescence as a function of the concentration of acceptor under different ionic conditions. For the lowest affinity state (1 mM Ca^{2+} in buffer; curve, ▲, in Fig. 2), the efficiency of FRET reached 100% at maximum surface coverage of acceptors. At the higher affinity states, the efficiency of FRET decreased to values of 80% and 48% for the 1 mM Mn^{2+} + 1 mM Ca^{2+}, and 1 mM Mn^{2+}-containing buffers, respectively (*curves*, ○, and ●, in Fig. 2).

Because the R18 membrane acceptor probe inserts into the cell plasma membrane with an unknown partition coefficient, we must estimate its surface density. To calibrate data from cells, the experimental values of acceptors per R_0^2 were determined by overlaying the quenching of a fluorescein lipid donor (F18) and the R18 acceptor on the calculated data from Wolber and Hudson. The experiments were conducted in such a way (time and temperature) as to minimize the redistribution of the two probes into intracellular membranes. Specifically, the use of F18 as a donor probe is complicated by the probe's tendency to undergo rapid flip-flop between the outer and inner leaflets as well as getting internalized in cytosolic space. To avoid the problem of flip-flop, we performed the calibration experiment using the F18 at 15°C. The results showed (Fig. 3 *A*) that the F18/R18 transfer and the LDV FITC/R18 transfer in the presence of Ca^{2+} to be equivalent to within experimental error. This means that the separation distance of the resting integrin was near 0 Å. The data shown in Figs. 2 and 3 *B* were collected at 37°C. We used the idea that the resting integrin was at the same height at both 15°C and 37°C to calibrate the surface density according to Wolber and Hudson and then overlaid the rest of the data set for the other ionic conditions.

The formalism of Wolber and Hudson (1979) (see Materials and Methods) was used to analyze the FRET data in terms of donor-acceptor separation distances. FRET is expressed in terms of relative donor emission (Q_{DA}/Q_D) as a function of the surface coverage of acceptors per unit area (acceptors per R_0^2, where R_0 for the fluorescein-rhodamine pair is 55 Å). The analysis provides insight both into the surface density of acceptors and the distance of nearest approach between donor and acceptors. The distance of closest approach between the donor probe (LDV-FITC) and R18 acceptor probes might be a reflection of several factors: the size of a protein or conformation, the distance of the donor above the membrane, or the presence of a boundary lipid which excludes the acceptor. It is important to note that the FRET analysis used here does not distinguish between lateral and vertical separation distances. The consequences

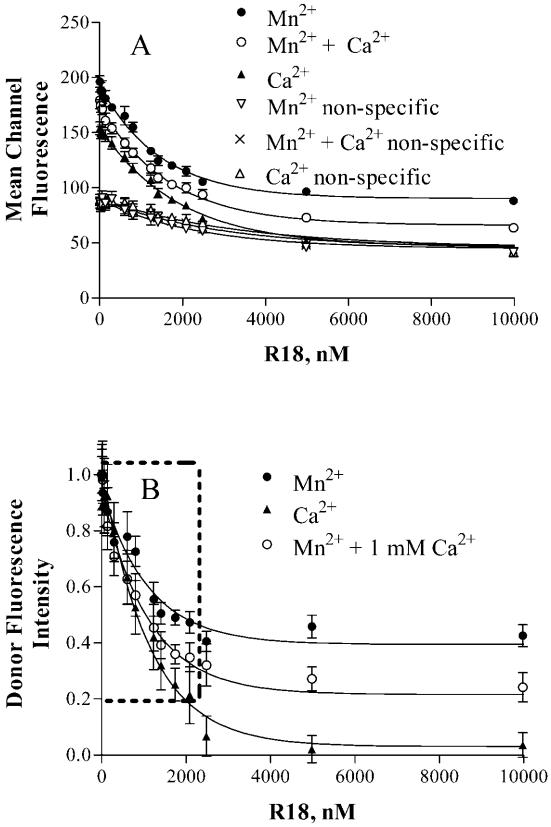

FIGURE 2 Energy transfer measurements on cells between LDV-FITC donor and R18 acceptor. (*A*) Fluorescent intensity measurements were made as a function of R18 concentration under three different cation conditions (1 mM Mn^{2+}, ●; 1 mM Mn^{2+} + 1 mM Ca^{2+}, ○; and 1 mM Ca^{2+}, ▲). Quenching data are plotted for total and nonspecific LDV-FITC binding conditions. Nonspecific binding was determined by measuring fluorescence associated with cells in the presence of a 500-fold excess of LDV unlabeled peptide. The FRET data were obtained using U937 cells equilibrated with 100 nM of LDV-FITC with or without 50 μM LDV unlabeled peptide. Samples were incubated with increasing concentrations of R18 (up to 20 μM) for 1 min and the green FITC fluorescence was measured using a Becton-Dickinson FACScan flow cytometer (Sunnyvale, CA). Data are plotted as mean channel fluorescence vs. concentration of R18. (*B*) The data from Fig. 2 *A* replotted as relative donor fluorescence intensity versus R18 concentration for different affinity states of the $\alpha_4\beta_1$-integrin. The values corresponding to nonspecific binding were subtracted and the data were normalized. One representative experiment out of five is shown. Data points represent means ± SE of the mean. Because the Wolber and Hudson model is only valid for acceptor densities of ≤0.5 acceptors/R_0^2, the analysis of the representative data in Fig. 2 is truncated. Thus the derived data shown in Fig. 3 represents the analysis of the data shown in the box as limited by the FRET model.

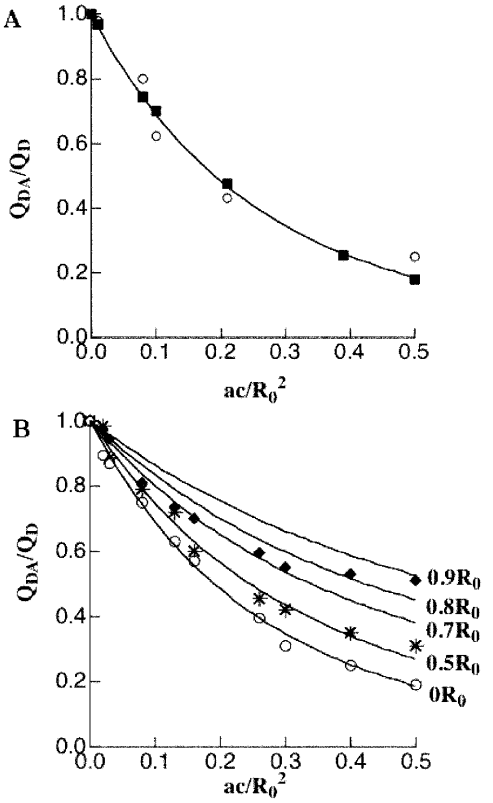

FIGURE 3 Calibration of acceptor surface density and distance of separation. The relative quantum yield, Q_{DA}/Q_D is plotted vs. acceptors/R_0^2 (Eq. 1) for randomly oriented donors and acceptors on lipid membranes. Q_{DA} is the donor quantum yield in the presence of acceptors and Q_D is the quantum yield in the absence of acceptors. (*A*) Determination of lateral energy transfer as a function of acceptor surface density calculated according to Wolber and Hudson (—). The FRET data corresponding to the F18/R18 membrane probes on U937 cells (■) and the LDV-FITC/R18 (○) at low affinity state of the integrin (1 mM Ca^{2+}) are overlaid. (*B*) Energy transfer as a function of donor distance of closest approach expressed in terms of R_0 according to the calculations of Wolber and Hudson. The surface densities are estimated for *B* from the results of *A*. Three affinity states are shown: 1 mM Mn^{2+}, ♦; 1 mM Mn^{2+} + 1 mM Ca^{2+}, ⋆; and 1 mM Ca^{2+}, ○.

of this limitation and applicability of this FRET model to our analysis will be developed in the Discussion section.

Because the Wolber and Hudson model is only valid for acceptor densities ≤ 0.5 acceptors/R_0^2, the analysis of the data in Fig. 2 is truncated. Thus the derived data shown in Fig. 3 represents the analysis of the data shown in the box as limited by the FRET model. Fig. 3 *B* shows the same treatment of FRET data for the three divalent cation-regulated affinity states. Whereas the lowest affinity state exhibits the highest quenching, the higher affinity states exhibit less efficient quenching (Table 2). Based on the calibration curve of Fig. 3 *A* and the calculated donor-acceptor distances from Wolber and Hudson (1979), the lowest affinity state of the integrin exhibits FRET similar to that expected if it were located much less than R_0 from the quencher, i.e., near the membrane surface. The separation distance for the highest affinity conformation is at a distance comparable to R_0, whereas the middle conformation lies at an intermediate distance.

For the various conditions under which FRET was measured, it is useful to comment on the factors that may affect the magnitude of R_0. The components of R_0 that might be sensitive to changes in the affinity state are the donor quantum yield and the orientation factor (Q_D and κ^2 in Eq. 2). Previous measurements showed that maximal ligand binding

TABLE 2 Separation distances between LDV-FITC bound to the α_4-integrin and the cell membrane surface

Affinity state	Maximal FRET efficiency (E, %)	Separation distance (fraction of R_0)*
1 mM Mn^{2+} + 3 mM DTT*	35	1.04–1.56
1 mM Mn^{2+}	48	0.80–1.25
1 mM Mn^{2+} + 1 mM Ca^{2+}	80	0.45–0.91
1 mM Ca^{2+}	100	0.00–0.45
100 nM fMLFF	65–85	0.45–0.73†

*Based on calibration of acceptor surface densities for resting receptor in 1 mM Ca^{2+} and assigned to 0 Å separation distance. Twenty percent uncertainty in calibration leads to uncertainty in separation distance $\sim 0.5\,R_0$.
†Uncertainty arises from the uncertainty of FRET efficiency.

(site number and its associated fluorescence) is independent of affinity state, suggesting that Q_D is invariant. (Chigaev et al., 2003). Two important limiting values of κ^2 in membranes are 0.667 and 0.476 corresponding to the randomization of donor-acceptor orientation by rotational diffusion of donors and acceptors before FRET, and the static randomization of donor-acceptor orientations, that otherwise remain constant during the lifetime of the donor (Lakowicz 1999). These limiting values of κ^2 produce a variation in the value of R_0 of ~5% and would change the slopes of the quenching curves by 10% or less.

Integrin conformation is regulated by inside-out signaling

Integrin affinity is known to be regulated by inside-out signaling by intracellular pathways (Hughes and Pfaff, 1998; Shimaoka et al., 2002). The signaling occurs through the cytoplasmic domain and rapidly activates ligand binding and the proposed conformational changes (Shimaoka et al., 2002). To determine whether the integrin conformation could be affected by the inside-out signaling, we used the human monoblastoid cell line U937 stably transfected with the wild-type formyl peptide receptor or the receptor mutant ΔST, which lacks all serines and threonines in the C-terminal tail and therefore does not desensitize (Prossnitz, 1997). Previously, we showed that the affinity change could be detected on live cells in response to the activation of several receptors (Chigaev et al., 2001). Here, changes in the efficiency of FRET were detected (Fig. 4), and the time course of these changes for two different mutants of the formyl peptide receptor coincides with the time course of the affinity changes, measured by the peptide binding. As these experiments were performed near ligand saturation, the alteration in the signal under FRET conditions could not be attributed to a change in ligand binding affinity (*curve*, —, in Fig. 4 *A*), and is thus most likely related to a change in conformation. The nondesensitizing mutant ΔST signaled over a longer duration than the wild-type receptor, as was shown before for the affinity change (Chigaev et al., 2001). The magnitude of the energy transfer for the ''physiologically activated state of the receptor'' therefore was similar to the intermediate affinity receptor state formed by divalent cations with excess Ca^{2+} (Chigaev et al., 2001).

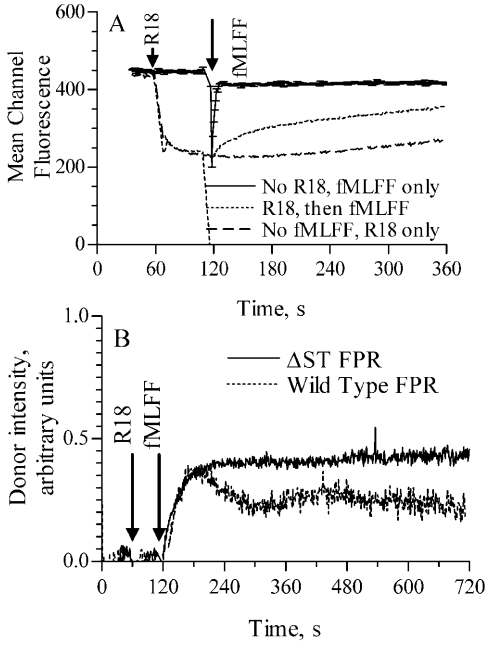

FIGURE 4 Real-time FRET experiments with physiological integrin activation. U937 cells stably transfected with the nondesensitizing mutant (ΔST) of formyl peptide receptor (FPR) were preincubated with 100 nM LDV-FITC peptide to saturate low affinity sites of the integrin in a buffer containing 1.5 mM $CaCl_2$ and 1 mM $MgCl_2$. Next, the LDV-FITC fluorescence was quenched after octadecyl rhodamine B addition (R18, 10 μM). Cells were then activated using formyl peptide (fMLFF, 100 nM) and the unquenching reaction was followed. (*A*) Data plotted as mean channel fluorescence versus time for three conditions: quenched, - - - ; quenched and stimulated, ··· ; and unquenched and stimulated, —. The unquenched control shows that no additional LDV-FITC binding is detected after fMLFF addition to contribute to the quenching analysis. (*B*) U937 cells transfected with wild-type formyl peptide receptor (···) or with the nondesensitizing mutant ΔST (—) were treated as described in Fig. 3 *A*. Data are replotted by subtracting the baseline data from unstimulated cells and normalizing to the unquenched fluorescence value of 1.0 before the addition of R18 and the quenched value of 0 caused by the addition of 10 μM R18. Because the formyl peptide receptor mutant ΔST does not desensitize, the α_4-integrin remains in a state of the constant affinity (Chigaev et al., 2001). The drift in the baseline quenching of Fig. 4 may be a result of R18 redistribution into inner membrane with a half-time of tens of minutes.

It is worth commenting on the characteristics of the two curves denoted by (—) and (- - -) in Fig. 4. In the first curve, addition of an aliquot of a high concentration (2 μL 10^{-4} M in DMSO) of fMLFF apparently results in a 20% drop in the intensity of the LDV-FITC. This appears to be associated with an effect of fMLFF on the nonspecific fluorescence signal (background rather than receptor binding of LDV-FITC, data not shown) but the mechanism has not been determined. However, since this does not occur when Mn^{2+} cations are used, this behavior has minimal impact on our model FRET determinations. The second curve appears to gradually drift upwards in time. As R18 may flip-flop

between the outer and inner leaflets of the plasma membrane and be internalized as well, a reduction in acceptor density in the outer leaflet would result in the gradual diminution of FRET over time, with a half-time of ~10 min.

Integrin molecules and R18 do not detectably segregate upon affinity regulation by divalent cations

We next used confocal microscopy to test whether cell treatment affects the gross distribution of donor (LDV-FITC) and acceptor (R18) molecules on the cell surface. The specificity of the LDV-FITC fluorescence was tested using confocal microscopy with 500-fold excess of the unlabeled LDV peptide derivative (compare Fig. 5, *c* and *d*). We found that the surface distribution of the α_4-integrin on U937 cells was relatively diffuse. Small uneven surface distribution of the fluorescence on the cell surface (*arrows*, Fig. 5 *c*) often described as ''integrin clustering,'' corresponds to the sites of microvilli, which can be seen on the DIC image (*arrows*, Fig. 5 *a*). The presence of an ''extra'' amount of the plasma membrane in these areas may account for the additional fluorescence intensity. It was also shown that on lymphocytes that $\alpha_4\beta_7$-integrin is highly concentrated on microvillus sites, whereas the β_2-integrin LFA-1 is excluded from villi (Berlin et al., 1995).

Next, we examined the ability of divalent ions to affect the distribution of LDV-FITC (FRET donor) and R18 molecules (FRET acceptors). U937 cells were stained with R18 or LDV-FITC in buffers containing different concentrations of Ca^{2+} and Mn^{2+} (see Materials and Methods). As expected, there was no segregation of R18 and LDV-FITC and no detectable difference in the distribution of R18 or LDV-FITC between U937 cells, incubated in buffers with varying concentrations of divalent cations (Fig. 6).

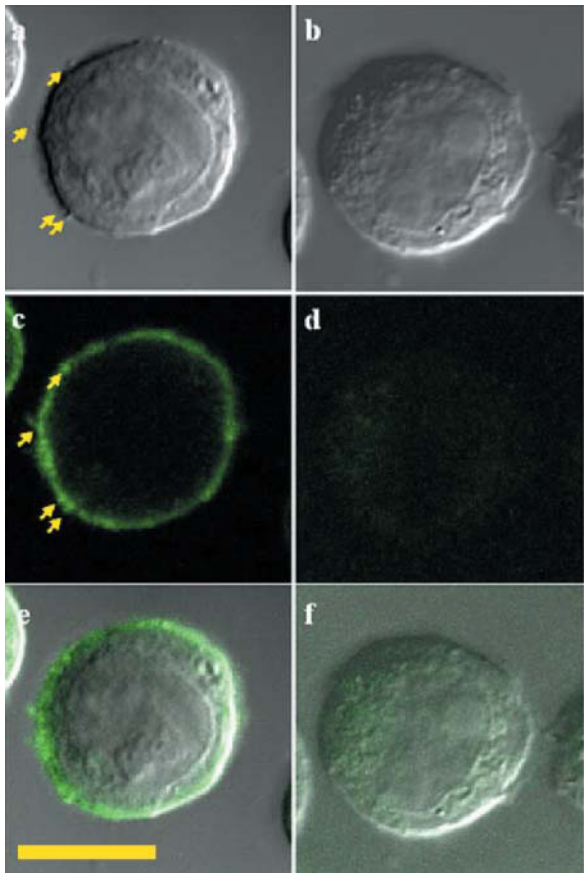

FIGURE 5 Specificity of LDV-FITC binding to U937 cells. U937 cells were incubated with 100 nM LDV-FITC in presence (*b*, *d*, and *f*) or absence (*a*, *c*, and *e*) of 50 μM of LDV blocking peptide, fixed overnight with 2% ice-cold PFA. (*a* and *b*) DIC image, (*c* and *d*) LDV-FITC fluorescence, and (*e* and *f*) overlay. This experiment was repeated 3× and gave similar results. Bar is 10 μm.

α_4-Integrin and R18 do not form detectable clusters after formyl peptide receptor stimulation

Clustering of activated G-protein coupled receptors is a well-described phenomenon. Clustering is related to the receptor desensitization, and internalization (Pierce et al., 2002; Rockman et al., 2002). In contrast to the wild-type receptor, the ΔST mutant of FPR, does not desensitize and internalize (Prossnitz, 1997), providing an opportunity to compare FPR α_4-integrin and acceptor distribution. U937 cells transfected with ΔST mutant of FPR, stained with R18, and a saturating concentration of LDV-FITC, were stimulated with 20 nM

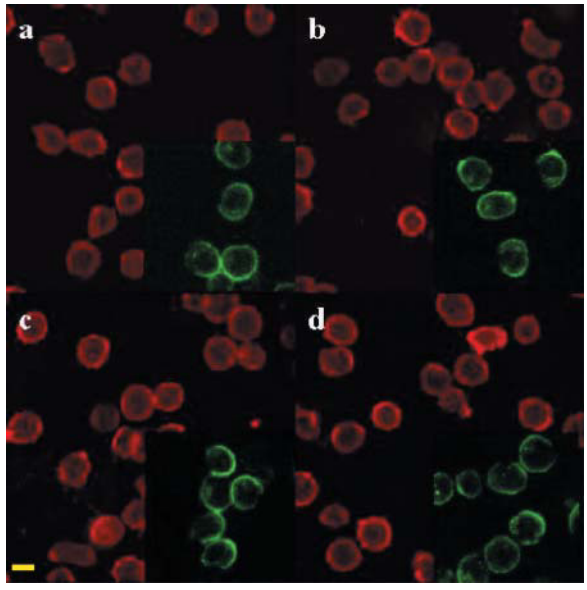

FIGURE 6 Distribution of LDV-FITC and R18 molecules is not altered in buffers with different concentration of divalent cations. U937 cells were preincubated in buffers containing 1 mM Ca^{2+} (*a*), 1 mM Mn^{2+} plus 10 mM Ca^{2+} (*b*), 1 mM Mn^{2+} plus 1 mM Ca^{2+} (*c*), and 1 mM Mn^{2+} (*d*) only. Cells were stained with 20 nM R18 for 1 min (*a–d*, *red*) or 100 nM LDV-FITC for 5 min (*a–d*, *green*) as for the FRET experiment. This experiment was repeated 4× and gave similar results. Bar is 10 μm.

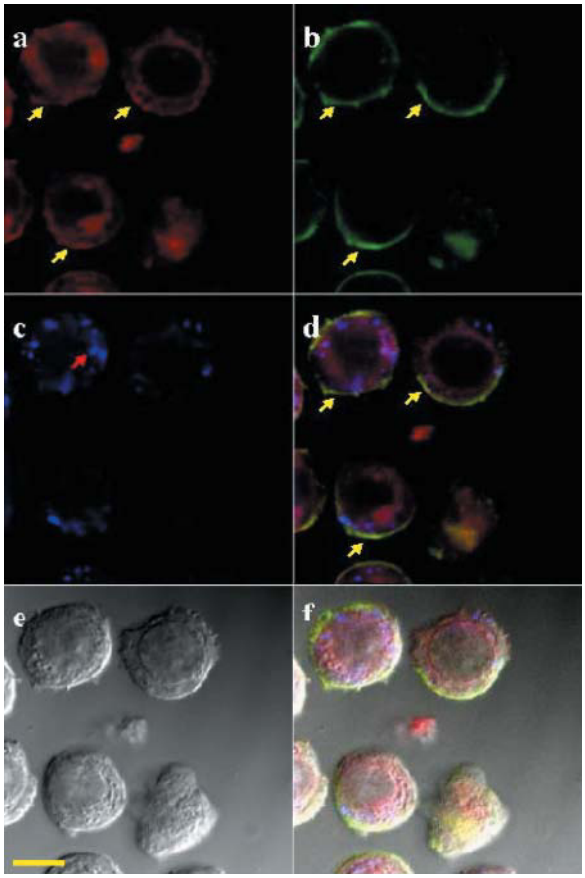

FIGURE 7 α_4-Integrin and R18 do not cluster after formyl peptide receptor stimulation. U937 cells transfected with ΔST mutant FPR were stained for 5 min with 100 nM LDV-FITC and 1 μM R18. Next, cells were stimulated with 20 nM fNle-Leu-Phe-Nle-Tyr-Lys-Alexa633 peptide, fixed, and analyzed by confocal microscopy. 3-min time-point is shown. (*a*) Membrane staining with R18, (*b*) LDV-FITC, (*c*) punctate structures of FPR, stained with fNle-Leu-Phe-Nle-Tyr-Lys-Alexa633, (*d*) overlay of *a, b*, and *c*, (*e*) DIC image, and (*f*) overlay of *a, b, c*, and *e*. No segregation or clustering of R18 (*a*) or LDV-FITC (*b*) with fNle-Leu-Phe-Nle-Tyr-Lys-Alexa633 (*c*, *red arrow*) was detected. Co-localization (*yellow*) of R18 incorporated into the plasma membrane and LDV-FITC is shown (*yellow arrows*). R18, as other lipophilic dyes do, internalizes (Molecular Probes); therefore all internal cell membranes are stained (*red* on *a*, *d*, and *f*). This experiment was repeated 4× and gave similar results. Bar is 10 μm.

fNle-Leu-Phe-Nle-Tyr-Lys-Alexa633 peptide and fixed in 2% paraformaldehyde. We found that 3–5 min after cell stimulation, the receptors segregated into the punctate structures (*red arrow*, Fig. 7 *c*), which were not co-localized with LDV-FITC bound to $\alpha_4\beta_1$-integrin (Fig. 7 *b*) and R18 membrane staining (Fig. 7 *a*). In contrast, segregation of LDV-FITC or R18 was not detected in our experiments. We also found a significant co-localization between LDV-FITC and R18 on the plasma membrane (*yellow arrows*, Fig. 7, *a, b*, and *d*). However, in addition to the staining of the plasma membrane, R18 (as other lipophilic dyes) does internalize over tens of minutes and stain all internal membranes (see *time course* in Fig. 4 *A*, showing loss of FRET over time). No significant internalization of LDV-FITC peptide was found during the time of the experiments. Thus, after cell stimulation through chemokine receptor the formyl peptide receptors form a punctate pattern on the cell surface, whereas the distribution of LDV-FITC donors and R18 acceptors remains unaffected.

DISCUSSION

Integrin conformations

Distinct conformations of integrin molecules have been visualized by electron microscopy (Du et al., 1993; Nermut et al., 1988; Takagi et al., 2001, 2002) and suggested by other methods (Chen et al., 1999b; Chigaev et al., 2001; Hughes and Pfaff, 1998). The model of a switchblade-like opening motion of integrin proposed by Beglova and coworkers is based on the finding that the activation-dependent and ligand-induced binding site epitopes of integrins are hidden in the bent conformation and exposed in the extended state (Beglova et al., 2002). This model implies a conformational change in response to integrin activation. Here using live cells constitutively expressing $\alpha_4\beta_1$-integrin (one of the most conformationally flexible among β_1-integrins; Bazzoni et al., 1998) we show that FRET reports a change in separation distance between the cell surface and the integrin binding pocket consistent with the argument that favors conformational change in the integrin. It is worth noting that the α_4-integrin subunit (CD49d) can form a heterodimer with the β_1 (CD29) or the β_7 subunit, thus forming VLA-4 ($\alpha_4\beta_1$) or $\alpha_4\beta_7$-integrin (Chan et al., 1992). VLA-4 recognizes the QIDS sequence in VCAM-1, and the LDV sequence in fibronectin. Similarly, the LDT sequence of MAdCAM-1 is essential for $\alpha_4\beta_7$-integrin binding (Fong et al., 1997; Viney et al., 1996). Thus, LDV can potentially bind to both types of integrins albeit with different affinities. As U937 cells express much more of the β_1 subunit than the β_7 subunit, the measurements described here predominantly reflects $\alpha_4\beta_1$ (Chigaev et al., 2001).

Distance of closest approach

A key finding is the occurrence of a progressive increase in α_4-integrin affinity, a decrease in ligand dissociation rate, and an increase in distance of closest approach (r_c) to the LDV-FITC binding site within the membrane as the integrin is activated. Based on the current knowledge about integrin activation and conformational changes, it is tempting to attribute the distances of closest approach as determined for the activated states to be solely due to the straightening of the stalks from a bent to an upright position. However, the FRET models used here do not, on their own, distinguish between lateral and vertical separation distances between the donor and acceptors. The plasma membrane is likely to be heterogeneous with lateral organization of proteins into

microdomains, such as lipid rafts and caveolae, mediating cell signaling and adhesion (Brown and London, 1998; Kenworthy, 2002; Simons and Ikonen, 1997; Simons and Toomre, 2000). Lipid rafts are associated with order-preferring lipid such as sphingolipids and cholesterol, whereas the nonraft regions tend to be composed of disorder-preferring lipids. Thus, different probes distribute according to their partition coefficients for a given environment. R18 belongs to the class of lipid probes that prefer disorder, and is generally excluded from lipid rafts (Vaz and Melo, 2001).

One argument that favors a lateral contribution is an apparent increase in r_c (i.e., upward deviation from Wolber-Hudson model) with increasing acceptor density (Fig. 3) as the affinity state is elevated. If integrin activation also involves separation of the stalks, closely apposed in the inactive state, the protein breadth could increase. Moreover, we cannot rule out the formation of nanoscopic clusters of integrins, which could potentially ''shield'' some LDV-FITC donors from acceptor quenching. However, several concepts also argue that the distance in Figs. 3 and 4 represent the vertical rather than the horizontal separation between donors and acceptors. Energy transfer is in general dependent upon acceptor rather than donor lateral distribution. Thus, one would have to hypothesize a ''clustering of the lipid probe acceptors'' induced by divalent cations. It is hard to imagine how donors and acceptors could become progressively laterally separated in Fig. 3 by the addition of specific cations. Moreover, under conditions of cell activation in Fig. 4, it has been suggested that lipid rafts might tend to segregate lipid probe or protein components (Leitinger and Hogg, 2002). However, $\alpha_4\beta_1$ VLA-4 and $\alpha_4\beta_7$-integrins have been shown to be excluded from lipid rafts (Shamri et al., 2002). We also show in Tables 1 and 2 that adding DTT to Mn^{2+} leads to slower ligand dissociation and increased separation distance. The dithiol compounds are well-known modulators of integrin-dependent adhesion (Edwards et al., 1995, 1998; Schwartz and Harlan, 1989). Thus, in three independent conditions that are highly unlikely to have similar consequences for lateral distribution of donor or acceptor, there is a correlation between ligand binding to the integrin and the distance of closest approach of R18 to the ligand binding site. The most probable cause is therefore a change in vertical separation attributable to extension of the integrin.

Because cellular lipid rafts are on the order of ≤ 0.1 μm (Anderson and Jacobson, 2002; Brown and London, 1998; Kenworthy, 2002; Kenworthy et al., 2000; Maxfield, 2002), and resolution of the microscope images is limited to ~ 0.1 μm, the lack of visible clusters in Figs. 5–7 does not rule out the existence of microdomains. An additional argument against the accumulation of the integrins into lipid rafts is based on the poor correlation between the real-time FRET response to activation of the integrin (Fig. 4) and the expected diffusion time of integrin traveling across the cell membrane toward a presumed microdomain. The half-time corresponding to the diminution of FRET due to activation of the integrin by a large excess of cations is <10 s (not shown), and <30 s (Fig. 4) for activation by inside-out signaling. In contrast, the diffusion time of integrin molecules to travel distances of a few microns (<3 μm) as measured by fluorescence recovery after photobleaching is on the order of minutes ($D \sim 10^{-10}$ cm^2 s^{-1}; see also Erb et al., 1997; Lippincott-Schwartz et al., 2001; Tsuruta et al., 2002). Taken together, the equilibrium and kinetic evidence suggest that the changes in FRET observed for the $\alpha_4\beta_1$-integrin are most likely due to conformational changes alone. By chemically attaching fluorescent tags to order preferring lipid probes such as GM1 ganglioside (Samsonov et al., 2001) it may be possible to probe the lipid domains that surround the receptors.

Uncertainties in vertical separation

The Wolber-Hudson model for FRET efficiency is based on the assumption that the integrin-bound donor moiety located above the membrane interacts with acceptor lipid probes that distribute uniformly in the membrane. The relevance of the model is supported by the close correlation between the F18/R18 calibration curve and the LDV-FITC/R18 FRET data for the resting receptor in Fig. 3. As the F18 and R18 probes are expected to have similar partition coefficients throughout the plasma membrane, the close match between these two curves suggests that the areas near the integrin are equally accessible to the lipid probe as the ''integrin free'' areas. Furthermore, the microscopy images shown in Figs. 6 and 7 indicate a relatively diffuse distribution of the integrin and the R18 (albeit limited in resolution to ~ 0.1 μm) with some co-localization.

However, several factors limit the reliability of the absolute values of the distances reported here. Since proteins typically occupy $\sim$20–50% of the membrane surface area (Saxton, 1989; Saxton and Jacobson, 1997), the assumption of random distribution of acceptors and their actual surface densities is an approximation. Second, the partition coefficient of the R18 lipid probes is likely to vary over different microregions of the laterally organized plasma membrane (Vaz and Melo, 2001). Models based on Monte Carlo simulations of FRET in ''crowded biological membranes'' have been published but do not appear to be applicable to the data presented here (Zimet et al., 1995). We have reported in Table 2 the ranges of separation distances based on uncertainties of $\sim$20% in local acceptor surface density. Deviations between the model and experimental data may result from imperfect calibration or segregation, particularly at high acceptor concentrations. Compared to uncertainties introduced by surface density, the impact of the uncertainty in κ^2 on R_0 is likely to be small because the R18 molecules are randomly oriented with respect to the binding pocket. In the binding pocket, LDV-FITC is likely to have at least limited motion, as there is torsional freedom in the FITC linkage and the amino acids

after LDV do not appear to contribute to overall ligand binding to the integrin (Lin et al., 1999).

Signaling and integrin activation

Placing the headpiece of the resting integrin near the membrane surface allows for an extension of the Mn^{2+} activated headpiece ~50 Å from the surface. This distance is approximately one-half that expected if the integrin molecule undergoes the conformational change from the fully folded to the fully extended conformation (compare Fig. 3, *H* and *I*, in Takagi et al., 2002). The activation of the integrin by inside-out signaling through a G-protein coupled receptor leads to the rapid unquenching of the donor fluorescence, which we interpret as a conformational change, that moves the molecule headpiece away from the lipid bilayer ~25 Å. In this case, the intermediate integrin conformational state induced by inside-out signaling would not be fully extended. The DTT treated and divalent activated integrin extends ~75 Å. The data support the notion that the conformational changes which promotes the extension has at the same time a progressive effect on the ligand binding affinity. The possibility that the effect of DTT is in the disulfide regulated integrin hinge region will be discussed elsewhere (Chigaev et al., unpublished results). Others have reported that the reduction of disulfide bonds within an integrin's cysteine-rich domain leads to global conformational changes of both α_{IIb}- and β_3-integrin subunits (Yan and Smith, 2001).

Our data do not at this time support a fully extended integrin conformation (see Fig. 6 *E* in Takagi et al., 2002). It is possible, therefore, that the fully extended conformation is short-lived or artificially generated by using soluble recombinant unclasped integrin molecules (Takagi et al., 2002). Alternatively, the fully extended conformation may exist at the moment of the engagement of the molecule by the natural ligand (e.g., VCAM-1 on endothelial cells) or may be a part of the cell braking system while it rolls on endothelium (Chen and Springer, 1999). These data therefore provide a mechanism to account for the notion of a catch-bond (Dembo et al., 1988). Such a bond would allow the forces of a cell-cell adhesive interaction to transduce a molecular extension and to induce a new conformation in the ligand-binding pocket that creates higher affinity, longer ligand residence time, and higher adhesive avidity.

Synergy in FRET in flow cytometry and microscopy

This study has employed a combination of flow cytometry, confocal microscopy, and FRET to examine the problem of conformational changes associated with integrin activation at cell surfaces. Generally, with FRET microscopy, it is possible to obtain quantitative temporal and spatial information about the organization, and interactions of cellular components such as proteins, lipids, enzymes, etc. (Kenworthy and Edidin, 1999; Kenworthy et al., 2000; Lippincott-Schwartz et al., 2001). However, steady-state microscopy measurements are typically affected by several sources of optical distortions that must be accounted for. These include background fluorescence, autofluorescence, photobleaching, direct excitation of acceptors, and the dependence of FRET on acceptor concentrations (Gordon et al., 1998). In the present work, the potential for very high fluorescence backgrounds from the real-time titration of lipid probes to cells would interfere with the effective use of microscopy. Flow cytometry is thus an effective alternative tool for quantitative FRET measurements in such an environment due to its intrinsic capacity to discriminate between free and cell-associated probes (Buranda et al., 1999; Nolan and Sklar, 1998; Sklar et al., 2002). Thus, in this work we have used flow cytometry for quantitation of FRET measurements and microscopy to visualize the lateral organization of cell membrane components. Using flow cytometry to resolve details of FRET in real-time (Fig. 4) and under steady-state conditions (Figs. 2 and 3) enabled us to define conditions under which no gross changes in the spatial distribution of donor and acceptor probes could be visualized after cell activation (Figs. 5–7).

We acknowledge the National Institutes of Health (grants P50 HL56384-06, IR01 RR14175, and IR24 CA88339-02 to L.A.S.; and AI36357 and AI43932 to E.R.P.) and the Dedicated Health Research Funds of the University of New Mexico School of Medicine (grant C-2192-RAC to T.B.) for support of this work. Images in this article were generated in the Fluorescence Microscopy Facility, which received support from the National Center for Research Resources 1 S10 RR14668, National Science Foundation MCB9982161, National Center for Research Resources P20 RR11830, National Cancer Institute R24 CA88339, the University of New Mexico Health Sciences Center, and the University of New Mexico Cancer Center.

REFERENCES

Alon, R., P. D. Kassner, M. W. Carr, E. B. Finger, M. E. Hemler, and T. A. Springer. 1995. The integrin VLA-4 supports tethering and rolling in flow on VCAM-1. *J. Cell Biol.* 128:1243–1253.

Anderson, R. G., and K. Jacobson. 2002. A role for lipid shells in targeting proteins to caveolae, rafts, and other lipid domains. *Science*. 296: 1821–1825.

Bazzoni, G., and M. E. Hemler. 1998. Are changes in integrin affinity and conformation overemphasized? *Trends Biochem. Sci.* 23:30–34.

Bazzoni, G., L. Ma, M. L. Blue, and M. E. Hemler. 1998. Divalent cations and ligands induce conformational changes that are highly divergent among β1-integrins. *J. Biol. Chem.* 273:6670–6678.

Beglova, N., S. C. Blacklow, J. Takagi, and T. A. Springer. 2002. Cysteine-rich module structure reveals a fulcrum for integrin rearrangement upon activation. *Nat. Struct. Biol.* 9:282–287.

Berlin, C., R. F. Bargatze, J. J. Campbell, U. H. von Andrian, M. C. Szabo, S. R. Hasslen, R. D. Nelson, E. L. Berg, S. L. Erlandsen, and E. C. Butcher. 1995. α4-integrins mediate lymphocyte attachment and rolling under physiologic flow. *Cell* 80:413–422.

Brown, D. A., and E. London. 1998. Functions of lipid rafts in biological membranes. *Annu. Rev. Cell Dev. Biol.* 14:111–136.

Buranda, T., G. P. Lopez, J. Keij, R. Harris, and L. A. Sklar. 1999. Peptides, antibodies, and FRET on beads in flow cytometry: a model

system using fluoresceinated and biotinylated β-endorphin. *Cytometry*. 37:21–31.

Chan, B. M., M. J. Elices, E. Murphy, and M. E. Hemler. 1992. Adhesion to vascular cell adhesion molecule 1 and fibronectin. Comparison of $\alpha4\beta1$ (VLA-4) and $\alpha4\beta7$ on the human B cell line JY. *J. Biol. Chem.* 267:8366–8370.

Chen, C., J. L. Mobley, O. Dwir, F. Shimron, V. Grabovsky, R. R. Lobb, Y. Shimizu, and R. Alon. 1999a. High affinity very late antigen-4 subsets expressed on T-cells are mandatory for spontaneous adhesion strengthening but not for rolling on VCAM-1 in shear flow. *J. Immunol.* 162:1084–1095.

Chen, L. L., A. Whitty, R. R. Lobb, S. P. Adams, and R. B. Pepinsky. 1999b. Multiple activation states of integrin $\alpha4\beta1$ detected through their different affinities for a small molecule ligand. *J. Biol. Chem.* 274:13167–13175.

Chen, S., and T. A. Springer. 1999. An automatic braking system that stabilizes leukocyte rolling by an increase in selectin bond number with shear. *J. Cell Biol.* 144:185–200.

Chigaev, A., A. M. Blenc, J. V. Braaten, N. Kumaraswamy, C. L. Kepley, R. P. Andrews, J. M. Oliver, B. S. Edwards, E. R. Prossnitz, R. S. Larson, and L. A. Sklar. 2001. Real-time analysis of the affinity regulation of $\alpha4$-integrin. The physiologically activated receptor is intermediate in affinity between resting and Mn^{2+} or antibody activation. *J. Biol. Chem.* 276:48670–48678.

Chigaev, A., G. Zwartz, S. W. Graves, D. C. Dwyer, H. Tsuji, T. D. Foutz, B. S. Edwards, E. R. Prossnitz, R. S. Larson, and L. A. Sklar. 2003. $\alpha4\beta1$-integrin affinity changes govern cell adhesion. *J. Biol. Chem.* 278:38174–38182.

Dembo, M., D. C. Torney, K. Saxman, and D. Hammer. 1988. The reaction-limited kinetics of membrane-to-surface adhesion and detachment. *Proc. R. Soc. Lond. B Biol. Sci.* 234:55–83.

Dewey, T. G., and G. G. Hammes. 1980. Calculation on fluorescence resonance energy transfer on surfaces. *Biophys. J.* 32:1023–1035.

Diamond, M. S., and T. A. Springer. 1994. The dynamic regulation of integrin adhesiveness. *Curr. Biol.* 4:506–517.

Doody, M. C., L. A. Sklar, H. J. Pownall, J. T. Sparrow, A. M. Gotto, Jr., and L. C. Smith. 1983. A simplified approach to resonance energy transfer in membranes, lipoproteins and spatially restricted systems. *Biophys. Chem.* 17:139–152.

Du, X., M. Gu, J. W. Weisel, C. Nagaswami, J. S. Bennett, R. Bowditch, and M. H. Ginsberg. 1993. Long range propagation of conformational changes in integrin αIIb $\beta3$. *J. Biol. Chem.* 268:23087–23092.

Dustin, M. L., and T. A. Springer. 1989. T-cell receptor cross-linking transiently stimulates adhesiveness through LFA-1. *Nature*. 341: 619–624.

Edwards, B. S., M. S. Curry, E. A. Southon, A. S. Chong, and L. H. Graf, Jr. 1995. Evidence for a dithiol-activated signaling pathway in natural killer cell avidity regulation of leukocyte function antigen-1: structural requirements and relationship to phorbol ester- and CD16-triggered pathways. *Blood*. 86:2288–2301.

Edwards, B. S., E. A. Southon, M. S. Curry, F. Salazar, J. M. Gale, M. K. Robinson, L. H. Graf, Jr., and J. L. Born. 1998. Oxidant inhibition of $\alpha L\beta2$-integrin adhesion: evidence for coordinate effects on conformation and cytoskeleton linkage. *J. Leukoc. Biol.* 63:190–202.

Erb, E. M., K. Tangemann, B. Bohrmann, B. Muller, and J. Engel. 1997. Integrin αIIb $\beta3$ reconstituted into lipid bilayers is nonclustered in its activated state but clusters after fibrinogen binding. *Biochemistry*. 36:7395–7402.

Faull, R. J., N. L. Kovach, J. M. Harlan, and M. H. Ginsberg. 1994. Stimulation of integrin-mediated adhesion of T-lymphocytes and monocytes: two mechanisms with divergent biological consequences. *J. Exp. Med.* 179:1307–1316.

Fong, S., S. Jones, M. E. Renz, H. H. Chiu, A. M. Ryan, L. G. Presta, and D. Jackson. 1997. Mucosal addressin cell adhesion molecule-1 (MAdCAM-1). Its binding motif for $\alpha4\beta7$ and role in experimental colitis. *Immunol. Res.* 16:299–311.

Fung, B. K., and L. Stryer. 1978. Surface density determination in membranes by fluorescence energy transfer. *Biochemistry*. 17: 5241–5248.

Gordon, G. W., G. Berry, X. H. Liang, B. Levine, and B. Herman. 1998. Quantitative fluorescence resonance energy transfer measurements using fluorescence microscopy. *Biophys. J.* 74:2702–2713.

Haugland, R. P. 2002. Handbook of Fluorescent Probes and Research Chemicals. Molecular Probes, Eugene, OR.

Hu, D. D., C. F. Barbas, and J. W. Smith. 1996. An allosteric Ca^{2+} binding site on the $\beta3$-integrins that regulates the dissociation rate for RGD ligands. *J. Biol. Chem.* 271:21745–21751.

Hughes, P. E., and M. Pfaff. 1998. Integrin affinity modulation. *Trends Cell Biol.* 8:359–364.

Humphries, M. J. 1996. Integrin activation: the link between ligand binding and signal transduction. *Curr. Opin. Cell Biol.* 8:632–640.

Humphries, M. J. 2000. Integrin structure. *Biochem. Soc. Trans.* 28: 311–339.

Hynes, R. O. 1992. Integrins: versatility, modulation, and signaling in cell adhesion. *Cell*. 69:11–25.

Kenworthy, A. 2002. Peering inside lipid rafts and caveolae. *Trends Biochem. Sci.* 27:435–437.

Kenworthy, A. K., and M. Edidin. 1999. Imaging fluorescence resonance energy transfer as probe of membrane organization and molecular associations of GPI-anchored proteins. *Methods Mol. Biol.* 116:37–49.

Kenworthy, A. K., N. Petranova, and M. Edidin. 2000. High-resolution FRET microscopy of cholera toxin B-subunit and GPI-anchored proteins in cell plasma membranes. *Mol. Biol. Cell*. 11:1645–1655.

Kew, R. R., T. Peng, S. J. DiMartino, D. Madhavan, S. J. Weinman, D. Cheng, and E. R. Prossnitz. 1997. Undifferentiated U937 cells transfected with chemoattractant receptors: a model system to investigate chemotactic mechanisms and receptor structure/function relationships. *J. Leukoc. Biol.* 61:329–337.

Lakowicz, J. R. 1999. Principles of Fluorescence Spectroscopy. Plenum Press, New York.

Leitinger, B., and N. Hogg. 2002. The involvement of lipid rafts in the regulation of integrin function. *J. Cell Sci.* 115:963–972.

Lin, K., H. S. Ateeq, S. H. Hsiung, L. T. Chong, C. N. Zimmerman, A. Castro, W. C. Lee, C. E. Hammond, S. Kalkunte, L. L. Chen, R. B. Pepinsky, D. R. Leone, A. G. Sprague, W. M. Abraham, A. Gill, R. R. Lobb, and S. P. Adams. 1999. Selective, tight-binding inhibitors of integrin $\alpha4\beta1$ that inhibit allergic airway responses. *J. Med. Chem.* 42:920–934.

Lippincott-Schwartz, J., E. Snapp, and A. Kenworthy. 2001. Studying protein dynamics in living cells. *Nat. Rev. Mol. Cell Biol.* 2:444–456.

Loftus, J. C., J. W. Smith, and M. H. Ginsberg. 1994. Integrin-mediated cell adhesion: the extracellular face. *J. Biol. Chem.* 269:25235–25238.

Lu, C., M. Ferzly, J. Takagi, and T. A. Springer. 2001. Epitope mapping of antibodies to the C-terminal region of the integrin $\beta2$ subunit reveals regions that become exposed upon receptor activation. *J. Immunol.* 166:5629–5637.

Maxfield, F. R. 2002. Plasma membrane microdomains. *Curr. Opin. Cell Biol.* 14:483–487.

Mould, A. P., S. K. Akiyama, and M. J. Humphries. 1995. Regulation of integrin $\alpha5\beta1$-fibronectin interactions by divalent cations. Evidence for distinct classes of binding sites for Mn^{2+}, Mg^{2+}, and Ca^{2+}. *J. Biol. Chem.* 270:26270–26277.

Nermut, M. V., N. M. Green, P. Eason, S. S. Yamada, and K. M. Yamada. 1988. Electron microscopy and structural model of human fibronectin receptor. *EMBO J.* 7:4093–4099.

Nolan, J. P., and L. A. Sklar. 1998. The emergence of flow cytometry for sensitive, real-time measurements of molecular interactions. *Nat. Biotechnol.* 16:633–638.

Pierce, K. L., R. T. Premont, and R. J. Lefkowitz. 2002. Seven-transmembrane receptors. *Nat. Rev. Mol. Cell Biol.* 3:639–650.

Prossnitz, E. R. 1997. Desensitization of *n*-formylpeptide receptor-mediated activation is dependent upon receptor phosphorylation. *J. Biol. Chem.* 272:15213–15219.

Rockman, H. A., W. J. Koch, and R. J. Lefkowitz. 2002. Seven-transmembrane-spanning receptors and heart function. *Nature*. 415: 206–212.

Samsonov, A. V., I. Mihalyov, and F. S. Cohen. 2001. Characterization of cholesterol-sphingomyelin domains and their dynamics in bilayer membranes. *Biophys. J.* 81:1486–1500.

Saxton, M. J. 1989. Lateral diffusion in an archipelago. Distance dependence of the diffusion coefficient. *Biophys. J.* 56:615–622.

Saxton, M. J., and K. Jacobson. 1997. Single-particle tracking: applications to membrane dynamics. *Annu. Rev. Biophys. Biomol. Struct.* 26: 373–399.

Schwartz, B. R., and J. M. Harlan. 1989. Sulfhydryl reducing agents promote neutrophil adherence without increasing surface expression of CD11b/CD18 (Mac^{-1}, Mo^{1}). *Biochem. Biophys. Res. Commun.* 165: 51–57.

Shamri, R., V. Grabovsky, S. W. Feigelson, O. Dwir, Y. Van Kooyk, and R. Alon. 2002. Chemokine stimulation of lymphocyte α4-integrin avidity but not of leukocyte function-associated antigen-1 avidity to endothelial ligands under shear flow requires cholesterol membrane rafts. *J. Biol. Chem.* 277:40027–40035.

Shimaoka, M., J. Takagi, and T. A. Springer. 2002. Conformational regulation of integrin structure and function. *Annu. Rev. Biophys. Biomol. Struct.* 31:485–516.

Simons, K., and E. Ikonen. 1997. Functional rafts in cell membranes. *Nature*. 387:569–572.

Simons, K., and D. Toomre. 2000. Lipid rafts and signal transduction. *Nat. Rev. Mol. Cell Biol.* 1:31–39.

Sklar, L. A., M. C. Doody, A. M. Gotto, Jr., and H. J. Pownall. 1980. Serum lipoprotein structure: resonance energy transfer localization of fluorescent lipid probes. *Biochemistry.* 19:1294–1301.

Sklar, L. A., B. S. Edwards, S. W. Graves, J. P. Nolan, and E. R. Prossnitz. 2002. Flow cytometric analysis of ligand-receptor interactions and molecular assemblies. *Annu. Rev. Biophys. Biomol. Struct.* 31:97–119.

Stewart, M., and N. Hogg. 1996. Regulation of leukocyte integrin function: affinity vs. avidity. *J. Cell. Biochem.* 61:554–561.

Takagi, J., H. P. Erickson, and T. A. Springer. 2001. C-terminal opening mimics ''inside-out'' activation of integrin $\alpha5\beta1$. *Nat. Struct. Biol.* 8:412–416.

Takagi, J., B. M. Petre, T. Walz, and T. A. Springer. 2002. Global conformational rearrangements in integrin extracellular domains in outside-in and inside-out signaling. *Cell.* 110:599–611.

Tsuruta, D., M. Gonzales, S. B. Hopkinson, C. Otey, S. Khuon, R. D. Goldman, and J. C. Jones. 2002. Microfilament-dependent movement of the β3-integrin subunit within focal contacts of endothelial cells. *FASEB J.* 16:866–868.

Van Kooyk, Y., S. J. van Vliet, and C. G. Figdor. 1999. The actin cytoskeleton regulates LFA-1 ligand binding through avidity rather than affinity changes. *J. Biol. Chem.* 274:26869–26877.

Vaz, W. L. C., and E. Melo. 2001. Fluorescence spectroscopic studies on phase heterogeneity in lipid bilayer membranes. *J. Fluor.* 11:255–271.

Viney, J. L., S. Jones, H. H. Chiu, B. Lagrimas, M. E. Renz, L. G. Presta, D. Jackson, K. J. Hillan, S. Lew, and S. Fong. 1996. Mucosal addressin cell adhesion molecule-1: a structural and functional analysis demarcates the integrin binding motif. *J. Immunol.* 157:2488–2497.

Wolber, P. K., and B. S. Hudson. 1979. An analytic solution to the Förster energy transfer problem in two dimensions. *Biophys. J.* 28:197–210.

Xiong, J. P., T. Stehle, B. Diefenbach, R. Zhang, R. Dunker, D. L. Scott, A. Joachimiak, S. L. Goodman, and M. A. Arnaout. 2001. Crystal structure of the extracellular segment of integrin $\alpha_V\beta3$. *Science*. 294:339–345.

Yan, B., and J. W. Smith. 2001. Mechanism of integrin activation by disulfide bond reduction. *Biochemistry.* 40:8861–8867.

Zimet, D. B., B. J. Thevenin, A. S. Verkman, S. B. Shohet, and J. R. Abney. 1995. Calculation of resonance energy transfer in crowded biological membranes. *Biophys. J.* 68:1592–1603.